Nanocrystallization and amorphization induced by reactive nitrogen sputtering in iron and permalloy

Rachana Gupta and Mukul Gupta*
Laboratory for Neutron Scattering, ETHZ & PSI, Paul Scherrer Institut, Villigen, CH-5232, Switzerland
(Received 22 December 2004; published 8 July 2005)

Thin films of iron and permalloy ($Ni_{80}Fe_{20}$) were prepared using an $Ar+N_2$ mixture with a magnetron sputtering technique at ambient temperature. The nitrogen partial pressure during the sputtering process was varied in the range of $0 \leqslant R_{N_2} \leqslant 100\%$, keeping the total gas flow at constant. At lower nitrogen pressures ($R_{N_2} \leqslant 33\%$), both Fe and NiFe first form a nanocrystalline structure, and an increase in R_{N_2} results in the formation of an amorphous structure. At intermediate nitrogen partial pressures, nitrides of Fe and NiFe were obtained, while at even higher nitrogen partial pressures, nitrides themselves became nanocrystalline or amorphous. The surface, structural, and magnetic properties of the deposited films were studied using x-ray reflection and diffraction, transmission electron microscopy, polarized neutron reflectivity, and using a dc extraction magnetometer. The growth behavior for amorphous film was found to be different as compared with poly or nanocrystalline films. The soft-magnetic properties of FeN were improved on nanocrystallization, while those of NiFeN were degraded. A mechanism inducing nanocrystallization and amorphization in Fe and NiFe due to reactive nitrogen sputtering is discussed in the present article.

DOI: 10.1103/PhysRevB.72.024202 PACS number(s): 61.10.Kw, 81.15.Cd, 68.55.Jk, 68.60.Dv

I. INTRODUCTION

During recent years, nanostructured and amorphous thin films and multilayers of magnetic materials have attracted tremendous scientific and technological interest due to their unique properties compared to conventional crystalline materials.[1–4] In nanocrystalline materials, as the grain size decreases, there is a significant increase in the volume fraction of grain boundaries or interfaces. This characteristic strongly influences the chemical and physical properties of the material. In particular, a decrease in the grain size results in improved soft-magnetic properties. On the other hand, amorphous phases are expected to be free from grains and grain boundaries, which often results in a release of intrinsic stresses, a decrease in magnetic anisotropy, and a smoother surface or interface. Furthermore, grains or grain boundaries act like an active path for diffusion, and therefore atomic self-diffusion in amorphous phases is expected to be lower. Amorphous or nanograin thin films exhibit a short-range ordering in the microstructure, and their structural, mechanical, electrical, and magnetic properties often depend on the methods and conditions of preparation.[5–7] Various attempts have been made to achieve amorphization in binary or multicomponent metal-metal and metal-metalloid systems using different techniques such as rapid-melt quenching,[8] mechanical alloying,[9] hydrogenation,[10] pressure,[11] interdiffusion reaction,[12–14] and ion or electron irradiation.[15,16]

Quite recently, nitrogen reactive sputtering has also been used to achieve a nanocrystalline or amorphous phase.[17–20] In the sputtering process, the adatoms have energy of the order of a few tens of eV, and during condensation onto the substrate, adatoms are quenched and may form an amorphous or fine-grain structure. At the same time, when sputtered using low-Z reactive ions, e.g., nitrogen ions, they may occupy interstitial sites in the unit cell of sputtered species, causing a distortion of the unit cell. A combined effect of these situations may lead to a nanocrystalline or amorphous structure of the deposited film. In order to verify such a mechanism causing nanocrystallization or amorphization, two different materials, namely bcc Fe and fcc NiFe permalloy, were chosen for the present study. In earlier studies, Fe thin films were prepared using an $Ar+N_2$ gas mixture by magnetron sputtering,[21,22] rf sputtering,[23–25] pulsed laser deposition,[26–28] ion-beam enhanced deposition (IBED),[29] etc. The motivation of most of these studies was to obtain a nitrogen-poor $Fe_{16}N_2$ phase which possesses a very high magnetic moment.[30,31] In some of these studies, an amorphous or nanocrystalline phase of FeN was obtained at low nitrogen pressure.[23,24,29] However, a detailed investigation of the evolution of nanocrystalline or amorphous phases and a mechanism inducing nanocrystallization or amorphization was not studied. It is known that when heated, evaporated, ablated, or sputtered in a nitrogen environment or with a nitrogen ion, iron forms a microstructure with a variety of FeN alloys and compounds, including the recently discovered new-cubic-type nitrides.[21,27] Ferromagnetic nitrides of iron have received tremendous interest in magnetic functional devices.[32,33] On the other hand, the NiFe alloy with a composition of $Ni_{80}Fe_{20}$ is a well-known soft-magnetic alloy and is known as a permalloy. It forms a face-centered-cubic structure of the type Ni_3Fe. In a recent study by Chiba *et al.*,[34] NiFe nitrides were deposited using an rf sputtering technique for a nitrogen flow in the range of 5–30 %. A decrease in saturation magnetization is reported, however a detailed variation in microstructure with higher nitrogen content was not investigated.

In this work, our aim is to explore the structural and magnetic properties and growth behavior of the bcc Fe and fcc NiFe thin films prepared using reactive nitrogen sputtering in the whole nitrogen partial pressure range (0–100%). In an earlier study by Kawamura *et al.*,[35] thin films of NiN were studied. In the present case, it was found that both Fe and

 ©2005 The American Physical Society

NiFe form an amorphous or nanocrystalline phase of either the element or a nitride of them when sputtered with nitrogen-poor or -rich mixtures. Polycrystalline films containing a mixture of nitrides were obtained at intermediate gas pressures and below or above, the long-range order of either the pure metal or its nitrides is restricted, and a nanocrystalline or amorphous structure is obtained. On the basis of obtained results, the mechanism leading the breakdown of long-range order is discussed. In order to understand the physical properties of the formed amorphous phases, the crystallization process was studied after annealing the thin films in vacuum. It is known that amorphous films have a smoother surface due to the absence of grains and lattice defects; the growth behavior of an amorphous phase and for comparison of pure Fe and nanocrystalline FeN was studied. Magnetic properties of ferromagnetic films were studied using a dc extraction magnetometer, and in order to avoid diamagnetism of the substrate, the magnetic moment was also determined using polarized neutron reflectometry. The results of the above-mentioned studies are presented and discussed in this article.

II. EXPERIMENTAL METHODS

Thin films of Fe and permalloy ($Ni_{80}Fe_{20}$) were prepared by magnetron sputtering using a gas mixture of $Ar+N_2$. The nitrogen partial pressure, defined as $R_{N_2}=P_{N_2}/(P_{N_2}+P_{Ar})\times 100\%$, was varied at 0, 2, 5, 10, 20, 33, 50, 83, and 100% for Fe and 0, 5, 10, 20, 33, 50, 59, 83, and 100% for NiFe. The gas flows in the vacuum chamber were controlled using mass flow controllers and the total gas flow for sputtering was kept fixed at 10 cm^3/min. Circular targets of pure Fe or permalloy, 75 mm in diameter, were sputtered with the gas mixture. A constant sputtering power of 50 W was used in all depositions. Slits of width 80 mm were placed between the target and the substrate to restrict the plasma. The cathode (target) and the substrate were mounted parallel to each other at a distance of about 8 cm. Before depositions, a base vacuum of the order of 1×10^{-6} mbar was obtained and the vacuum chamber was flushed with Ar and N_2 gas so as to avoid contamination of other gases inside the vacuum chamber. The pressure during deposition was in the range of $(4-8)\times 10^{-3}$ mbar. The substrates were mounted below the targets and oscillated with respect to the central position of the target for better uniformity of the deposited samples. All the samples were deposited at room temperature (~298 K, without intentional heating) on float glass or Si [100] substrates (films used for annealing at high temperatures were deposited on Si substrates). Thin films for growth studies were deposited in a single sputtering run (for one composition) onto a glass substrate. The substrate was covered with a small slit of size 15 mm and exposed in the center for a different amount of time to obtain different thicknesses. The substrate was translated using a computer-controlled linear translation stage. The thicknesses of the films were determined using x-ray reflectivity (XRR) technique and the structure of the films was investigated using grazing-incidence x-ray diffraction (XRD) using Cu $K\alpha$ x rays. For all the measurements, the incident angle was kept fixed just above the critical angle of the film, to minimize the background due to diffraction of the substrate. The bulk magnetic measurements were performed using a dc extraction magnetometer with the magnetic field applied parallel to the plane of the film using a physical property measurement system (PPMS). In order to determine the magnetic moment of the films, independent of substrate magnetism or sample area, the polarized neutron reflectivity (PNR) measurements were performed at the saturation field of the samples. The measurements were performed at a fixed angle of incidence in the time-of-flight (TOF) mode at AMOR(SINQ/PSI).[36]

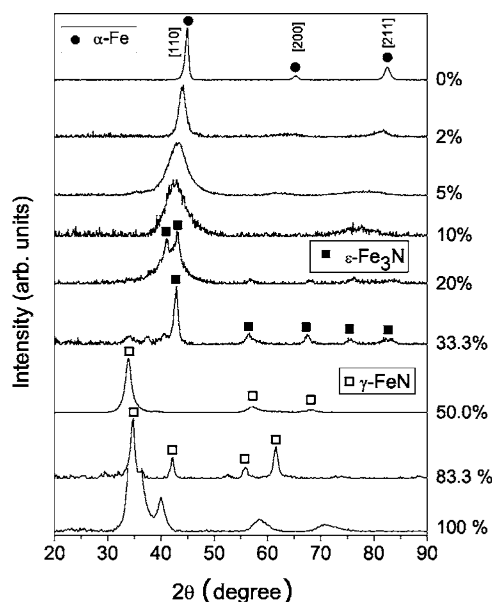

FIG. 1. Grazing incidence x-ray-diffraction pattern of FeN thin films prepared with different nitrogen partial pressure.

III. RESULTS AND DISCUSSION

A. Structural properties: FeN

Figure 1 shows the grazing-incidence XRD pattern of Fe films prepared with different nitrogen partial pressure. The film prepared with Ar gas only shows reflections corresponding to bcc α-Fe with orientation in the direction of the [110] plane. For the films prepared with 2–20 % nitrogen partial pressure (rest Ar), the XRD pattern shows a structure similar to bcc α-Fe, however all the peaks were broad and the peak positions were shifted to the lower angle side as compared to the XRD pattern of pure Fe film. The linewidth of the diffracted pattern can be used to calculate the grain size of the diffracting specimen in the direction perpendicular to the plane of the film using the Scherrer formula,[37] $t=0.9\lambda/b\cos\theta$, where t is the grain size, b is an angular width in terms of 2θ, θ is the Bragg angle, and λ is the wavelength of the radiation used. For the film prepared with Ar gas only, the average grain size was 13 ± 1 nm, while in the presence of 2% nitrogen partial pressure during sputtering it decreases to 6 ± 1 nm, about half of the value found without any nitrogen. This result indicates that even a presence of nitrogen as small as 2% significantly affects the

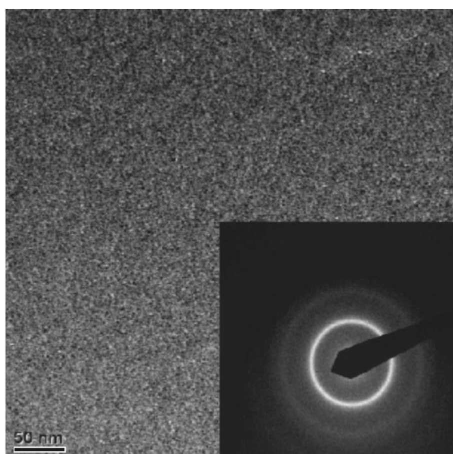

FIG. 2. TEM planar view of the sample prepared at 10% nitrogen partial pressure. The inset of the picture shows the electron-diffraction pattern.

growth of Fe crystals and restricts the long-range order. The positions of Bragg peaks for the sample prepared with 2% nitrogen were shifted to lower-angle side, indicating an increase in the interatomic spacing. The average interatomic distance can be estimated using the relation $a=1.23/2 \sin \theta$, where θ is taken to be the angle at the center of the peak, and the factor 1.23 is a geometric factor which rationalizes the nearest-neighbor distance with the spacing between "pseudo-close-packed planes."[38] Comparing the interatomic spacing for the film prepared without nitrogen and with 2% nitrogen, the average interatomic spacing was found to be expanded by 2%. On increasing the nitrogen partial pressure, the width of the reflections further increases and peak position continues to shift towards the lower angle side. At 5% and 10% nitrogen partial pressure, the linewidth of the peak becomes as large as 4°, which is close to the value found for conventional iron-based amorphous alloys.[3]

The amorphous nature of the film deposited at $R_{N_2}=10\%$ was confirmed with transmission electron microscopy (TEM). A thin film of thickness 70 nm was directly deposited on a carbon-coated TEM grid. Figure 2 shows a representative TEM micrograph along with the electron-diffraction pattern. Similar micrographs were observed throughout the plane of the film. The micrograph essentially showed a featureless structure and the electron-diffraction pattern showed a diffuse diffraction ring which confirms the amorphous nature of the film.

Figure 3 shows a plot of the average interatomic distance a as a function of increase in the nitrogen partial pressure in the range of 0–20 % for FeN and 0–33 % for NiFeN. As can be seen from the figure, with an increase in the amount of nitrogen, the interatomic spacing continues to increase. However, at 20% the broad hump overlaps with two sharp peaks. The positions of the sharp peaks correspond to the hcp ϵ-Fe_3N phase. And the overall structure can be considered as a mixture of amorphous bcc Fe along with the hcp ϵ-Fe_3N phase. At 33.3% nitrogen partial pressure, the structure changes completely and the ϵ-Fe_3N phase along with the ζ-Fe_2N phases were obtained. On further increasing the nitrogen partial pressure at 50%, the structure changes again

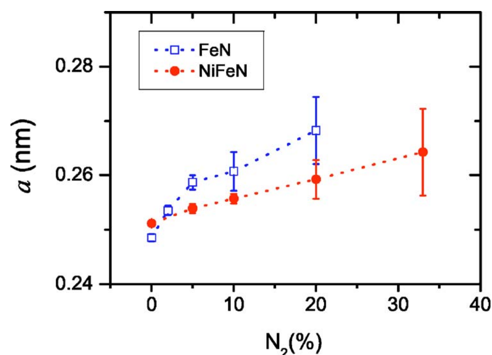

FIG. 3. (Color online) Interatomic spacing as a function of nitrogen partial pressure in FeN and NiFeN.

and reflections corresponding to new-cubic-type phase were obtained. It may be noted that the width of the Bragg peak at 34° is $(1.4° \pm 0.01°)$ corresponding to an average grain size of about 6 nm, which is an indication of the formation of a nanograin structure. At 83.3% nitrogen partial pressure, sharp peaks corresponding to the γ''-FeN phase were observed. On further increasing the nitrogen partial pressure to 100%, the peak widths again start increasing, indicating the reformation of a nanocrystalline structure.

B. Structural properties: NiFeN

The permalloy target was also sputtered with a mixture of $Ar+N_2$ by varying the nitrogen partial pressure in the range of 0–100 %. Figure 4 shows a grazing incidence x-ray-diffraction pattern of NiFeN thin films prepared at different nitrogen partial pressure. The film prepared with Ar gas only shows reflections corresponding to the permalloy phase as indexed in the figure. As the nitrogen partial pressure is increased, the reflection starts broadening and the reflection

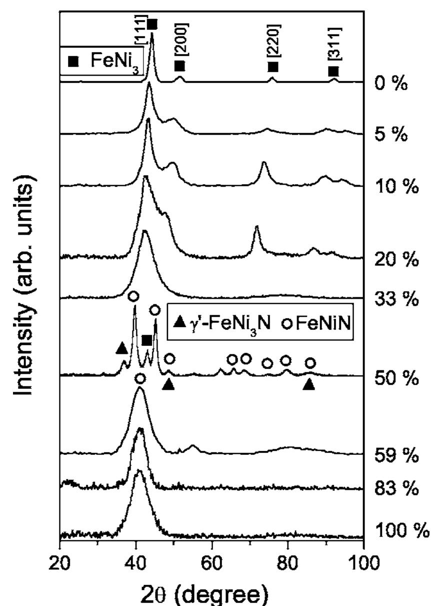

FIG. 4. Grazing incidence x-ray-diffraction pattern of NiFeN thin films prepared with different nitrogen partial pressure.

with indices [111] and [200] starts merging together. A clear shift in the positions of the Bragg peak is also evident. The grain size for the film sputtered with Ar only was 7 nm, which decreases to 3.5 nm after sputtering with 5% or 10% nitrogen. With a further increase in the nitrogen partial pressure, an amorphous phase appeared at 33%. As compared to FeN, the shifts in the positions of Bragg peaks were rather small (see Fig. 3). Also an overall increase in the interatomic distance at similar nitrogen pressure was smaller in NiFe as compared to Fe. A discussion related to this issue is given in Sec. IV. While comparing the observed results with that of NiN studied by Kawamura *et al.*,[35] a similar broadening and expansion of the unit cell of Ni was observed. On increasing the R_{N_2} to 50% with NiFe, the structure was changed completely and several peaks were observed in the XRD pattern. The phase identified at this pressure is a mixture of FeNiN $+\gamma'$-$FeNi_3N$. On further increasing R_{N_2} to 59% or above, a broad hump around $2\theta=40°$ appears along with faint reflections at higher angles. This hump appears to be an envelope of several reflections observed for the $R_{N_2}=50\%$ sample and indicates reamorphization of the polycrystalline permalloy nitride structures formed at $R_{N_2}=50\%$.

Nanocrystallization or amorphization induced by reactive nitrogen sputtering in Fe, Ni, and NiFe can be explained with a single mechanism. At low nitrogen partial pressures, nitrogen ions do not react with Fe, Ni, or NiFe and nitrogen is incorporated in the interstitial sites, making an expansion of the unit cell. At intermediate nitrogen pressure, a chemical reaction between nitrogen and Fe, Ni, or NiFe is favorable, which results in the formation of nitride phases. At still further higher nitrogen pressures, deformation of the formed nitride phase starts and the end structure is again nanocrystalline or amorphous. The detailed mechanism inducing nanocrystallization or amorphization is discussed in Sec. IV.

C. Crystallization behavior of amorphous films

From the observed XRD results, it is evident that when nitrogen partial pressure during sputtering is 5% and 10%, an amorphous phase of FeN was formed, while at 33% and above 50%, an amorphous NiFeN phase was formed. It would be interesting to study the crystallization behavior of these amorphous phases in order to understand their properties. Two sets of samples were chosen for crystallization studies: (i) Fe-rich, FeN samples prepared at $R_{N_2}=2$, 5, 10, and 20%, and (ii) N-rich, NiFeN samples prepared at $R_{N_2}=83\%$. These films were annealed in a vacuum furnace isochronally for 1 h at each temperature. In order to avoid the fluctuations in temperature, all four FeN films were annealed simultaneously in the vacuum furnace. Figures 5(a)–5(d) show the grazing incidence XRD pattern of annealed FeN films. It is interesting to observe that the films prepared with 2% and 5% nitrogen partial pressure were highly unstable, and even at 150 °C, Bragg peaks corresponding to α''-FeN appear in the XRD pattern. The film prepared with $R_{N_2}=10\%$ was found to be more stable and it remained amorphous up to an annealing temperature of 200 °C. On further annealing at 300 °C, the amorphous hump splits into three sharp peaks corresponding to the ϵ-Fe_2N_{1-z} phase, and at

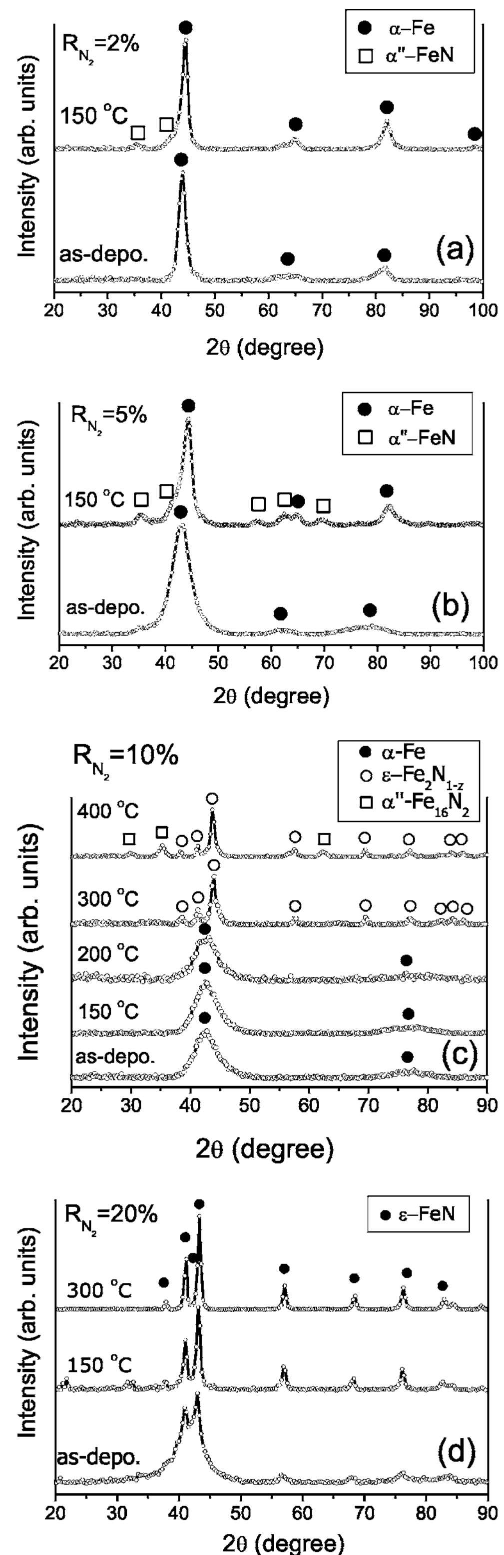

FIG. 5. Grazing incidence x-ray-diffraction pattern of FeN film prepared with 2% (a), 5% (b), 10% (c), and 20% (d), in the as-deposited state and after vacuum annealing at various temperatures. The films were annealed isochronally for 1 h.

400 °C, new peaks corresponding to the α''-$Fe_{16}N_2$ phase were observed. For the film prepared with $R_{N_2}=20\%$, the XRD pattern reveals a composite structure consisting of amorphous bcc Fe and ϵ-Fe_2N_{1-z} phase in the as-deposited

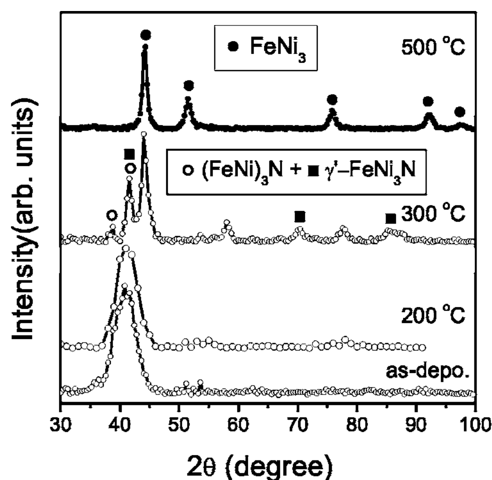

FIG. 6. Grazing incidence x-ray-diffraction pattern of NiFeN thin film prepared with 83% nitrogen partial pressure after annealing at different temperatures.

state, and after annealing at 150 °C, the structure crystallizes into an ϵ-Fe_2N_{1-z}. The observed crystallization behavior of the amorphous phase shows that the amorphous phase shows a better stability for the film prepared with $R_{N_2}=10\%$, and the films prepared either with higher or lower nitrogen are formed in a highly metastable state. Figure 6 shows a grazing incidence XRD pattern of the NiFeN film prepared at $R_{N_2}=83\%$, after annealing at different temperatures. As can be seen from the figure, up to an annealing temperature of 250 °C, no significant changes in the XRD pattern were observed, while after annealing at 350 °C, several peaks were observed. The most intense peaks correspond to the $(FeNi)_3N$ and γ'-$FeNi_3N$ phases. Smaller peaks at 53.6°, 58.2°, and 77.8° could not be identified. After further annealing at 500 °C, no nitride phase was observed, indicating outdiffusion of nitrogen.

The observed crystallization behavior of both amorphous FeN and NiFeN phases is different as compared to iron-based binary or multicomponent alloys. In conventional metal-metal amorphous alloys, generally crystallization occurs in two steps. In the first step, a nanocrystalline microstructure coexists with a parent amorphous phase, whereas in the second step an intermetallic compound along with a nanocrystalline phase precipitates out. The nominal reaction for such crystallization process had been given as follows: amorphous $\rightarrow \alpha+$amorphous $\rightarrow \alpha+\beta$, where α is the primary phase that precipitates out from the amorphous matrix and β is an intermetallic compound.[39,40] In the present case, however, crystallization takes place in a single step and annealing at temperatures above crystallization temperatures essentially results in nitrogen outdiffusion. The amorphous structure remained amorphous up to a certain annealing temperature and thereafter mixed nitride phases were observed. On further annealing due to nitrogen outdiffusion, pure metallic or nitrogen-poor phases were obtained.

D. Surface properties and growth behavior of FeN films

The thickness of FeN and NiFeN thin films deposited for $R_{N_2}=0-100\%$ was determined using an x-ray reflectivity technique. Since both FeN and NiFeN thin films were deposited in a similar manner, detailed surface and growth behavior of FeN thin films was investigated. Figure 7 shows an x-ray reflectivity pattern of FeN thin films prepared at different nitrogen partial pressures. The x-ray reflectivity pattern was fitted using a computer program[41] based on Parratt's formalism.[42] Oscillations due to total thickness of the films can be clearly seen in the reflectivity pattern. The thickness of the films was obtained after fitting the pattern and was found to be in the range of 90–100 nm. The fitted parameters are given in Table I. A detailed fitting of the pattern revealed that a thin layer with a density of about 50% of the bulk of the layers is formed on the surface. Such a layer may be formed due to "oxidation" of the surface when exposed to atmosphere. The thickness of this layer was typically 2–3 nm. It is interesting to see that the roughness of the film prepared with Ar gas only was 3.3 nm, which decreases to 2 nm at $R_{N_2}=2\%$, and was only 0.4 nm for $R_{N_2}=10\%$. At $R_{N_2}=20\%$ and 50%, the roughness again increases to 1 nm and at 83% again it decreases slightly. While looking at the microstructure of the deposited film obtained from XRD

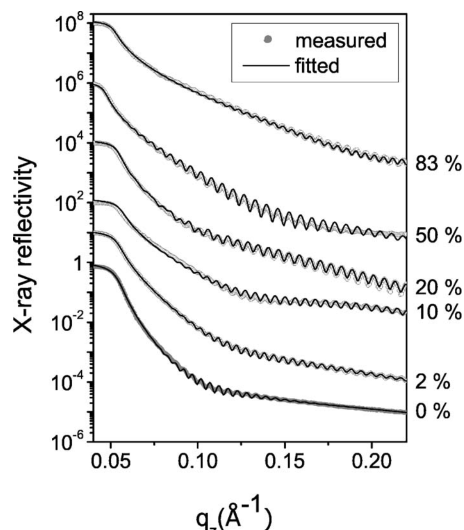

FIG. 7. X-ray reflectivity pattern of FeN thin films prepared with different nitrogen partial pressure. Scattered data (gray-shaded) represent experimental data and solid lines correspond to the theoretical model.

TABLE I. Fitted x-ray reflectivity parameters for FeN thin films prepared at different nitrogen partial pressures.

R_{N_2} (%)	Film thickness nm (±0.2)	Film roughness nm (±0.1)	Substrate roughness nm (±0.2)
0	103.5	3.3	0.6
2	105.4	2.0	0.6
10	101.6	0.4	0.6
20	98.3	1.0	0.6
50	93.5	1.0	0.6
83	113.5	0.8	0.6

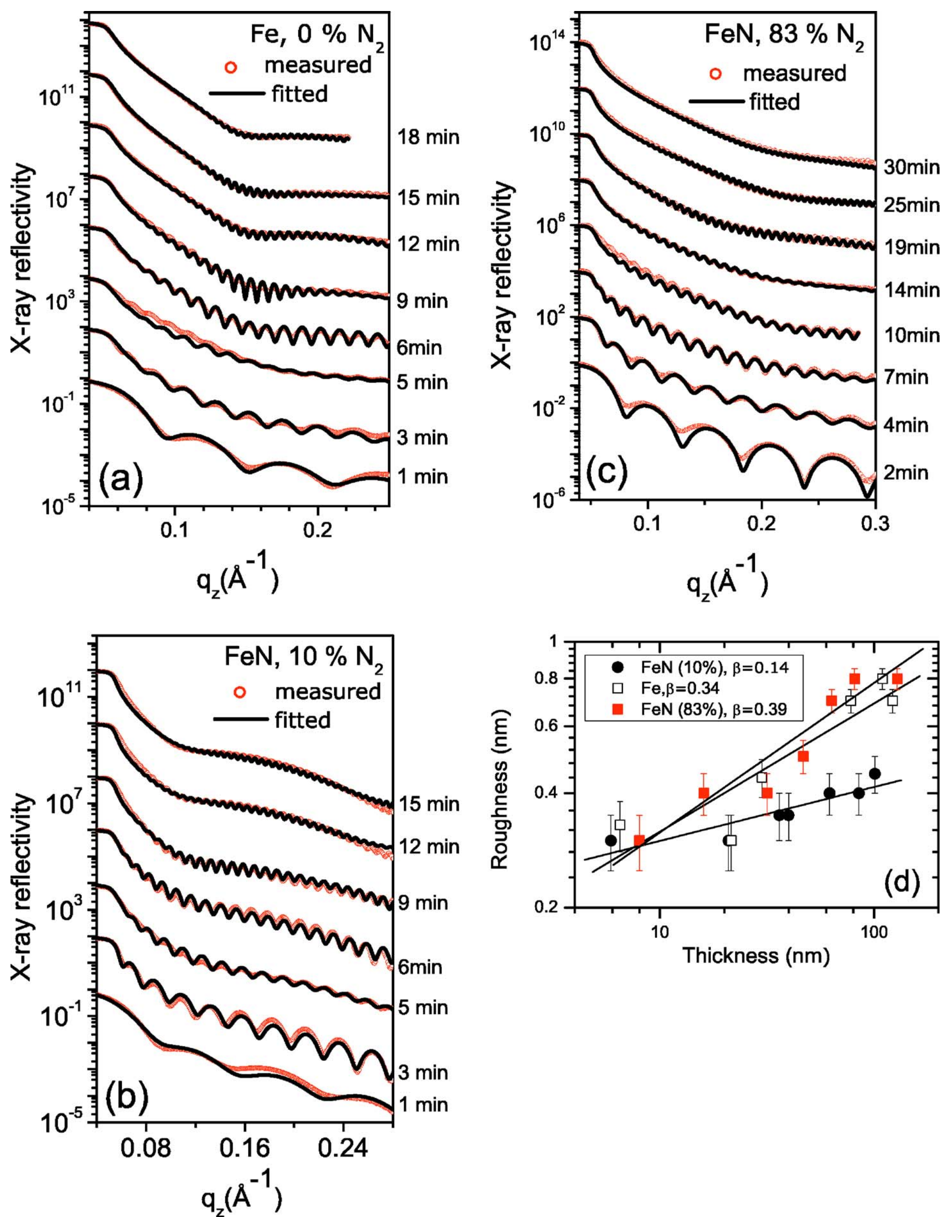

FIG. 8. (Color online) X-ray reflectivity pattern of pure Fe film (a), FeN film with 10% N (b), and FeN film with 83% nitrogen partial pressure (c). The evolution of film roughness with film thickness (d).

measurements, there is a clear indication that an amorphous phase is formed at lower and higher nitrogen partial pressures. A decrease in the roughness of film is not unexpected since the amorphous structure is free of grains and lattice defects, which may result in the formation of a smoother surface or interface. With the observed decrease in the roughness of the film for amorphous samples, it would be interesting to study the growth behavior of these films. For this purpose, a series of FeN thin films were deposited at R_{N_2} =0%, 10%, and 83%. In order to minimize the parameters influencing the growth of a thin film, all the films with one composition were prepared in a single sputtering run. For this purpose, the substrate was masked with a small slit of size 15 mm and all the films were prepared on a glass substrate by exposing the substrate for different times to the plasma at different positions on the substrate to obtain different thicknesses.

The films were prepared in the thickness range of 10–150 nm. X-ray reflectivity (XRR) measurements on all the films were performed in specular and off-specular modes. The offset in off-specular measurements was taken at the onset of the specular reflection peak in the rocking scan. This offset was 0.05°. The off-specular data were subtracted from the specular data to obtain the "true-specular" data. Figures 8(a)–8(c) show the XRR patterns of above-mentioned thin films. The patterns were fitted using a procedure as describe earlier. It was observed that for pure iron film, the surface roughness increases monotonically with an increase in the thickness, while for the amorphous FeN film the roughness of the film increases at a very slow rate. For the case when FeN forms a nanocrystalline nitride at R_{N_2}=83%, the surface roughness again shows an increase with the thickness. Previous studies have shown that the rms roughness (σ) exhibits a power-law behavior,[20,43] as a function of the film thickness, given as $\sigma \sim t^{\beta}$. Accordingly, a double logarithmic plot of the rms roughness of the films versus the film thickness should yield a linear relation. Figure 8(d) shows a plot rms roughness versus film thickness for the above-mentioned samples,

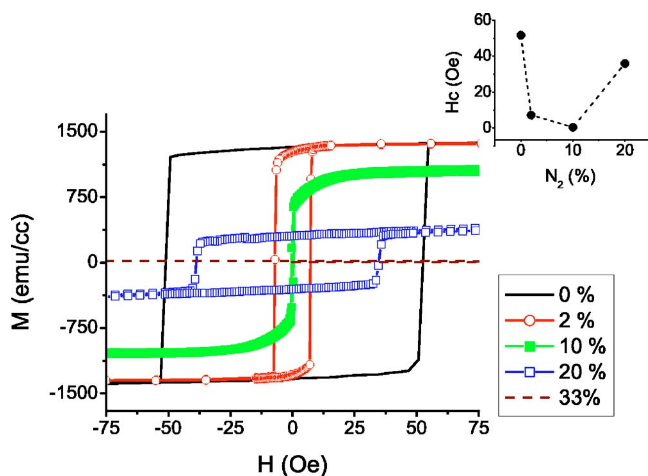

FIG. 9. (Color online) Magnetization measurements of FeN thin films prepared at different nitrogen partial pressures. The inset shows a variation in coercivity as a function of nitrogen partial pressure during sputtering.

and a straight line fit to the data yields the roughness growth exponent, β. For pure Fe film β=0.35, for amorphous FeN film prepared at R_{N_2}=10%, β=0.14, and for nanocrystalline FeN film prepared at R_{N_2}=83%, β=0.39. The value of β for amorphous FeN is very close to that obtained for amorphous SiO_2 (Ref. 44) and nitrogen-rich amorphous FeN prepared using ion-beam sputtering.[20] Under the various growth models described in the literature, it may be observed that for the values of the roughness growth exponent lying in the range of 0.1–0.25, the growth can be well described by the KPZ model, first introduced by Kardar, Parisi, and Zhang.[45] This type of growth process takes into account a random deposition and a limited relaxation of the particles at the surface. For the present case, the value of the amorphous sample lies well in this range, while for both pure Fe and nanocrystalline FeN, the value of β is higher. A higher value of β indicates non-KPZ-type growth, which is often observed for polycrystalline elements. The obtained results clearly show a different growth mechanism for amorphous film and support the argument that amorphous films yield smoother surfaces. It may be noted that the absolute roughnesses of the films prepared with smaller slits (15 mm) were smaller as compared with the larger slits (80 mm).

E. Bulk magnetization measurements of FeN and NiFeN films

Figure 9 shows the MH curve of the FeN samples prepared at different nitrogen partial pressure. For the film prepared with Ar gas only, the behavior is as expected for iron, and the value of saturation magnetization (Ms) was almost equal to the reported values for bulk Fe. For the sample prepared at R_{N_2}=2%, the MH loop shape changes to a typical soft-magnetic. While the value of saturation magnetization is almost equal to pure Fe, the MH curve shows a significant decrease in the value of coercivity (Hc). It may be noted that the average grain size (D) for pure Fe is about 13 nm, while for the sample prepared with 2% nitrogen partial pressure, the grain size reduces to 6 nm. A decrease in Hc in nanocrystalline ferromagnets is expected as envisaged in the random-anisotropy model (RAM).[46–48] It may be noted that the ferromagnetic exchange length (L_{ex}) for α-Fe is 15–23 nm.[49,50] For grain sizes $D < L_{ex}$, Hc decreases with a decrease in grain size by D^6. A reduction in grain size below ferromagnetic exchange length allows exchange coupling between the neighboring grains and results in a reduced effective anisotropy $\langle K\rangle$. In the present case, however, the decrease in Hc was not found to vary with D^6, rather it follows D^{2-3}-type behavior. Since in the present case the thickness of the films is small, it is likely that effective averaging would be only in the plane (area) of the film. In this situation, the ferromagnetic correlation volume would be proportional to L_{ex}^2 only, in contrast to L_{ex}^3 in the case of bulk materials. This would reduce the number of grains over which the averaging is done, and therefore a reduction in the magnetic anisotropy and Hc is not expected to vary as D^6, as observed in nanocrystalline ribbons or powders. Assuming averaging over $N=(L_{ex}/D)^2$ number of grains, the effective anisotropy would be

$$\langle K\rangle = \frac{K_1^2 D^2}{A}, \tag{1}$$

where K_1 is the magnetocrystalline anisotropy of the grains and A is the exchange stiffness. This would mean that in the case of a thin film, Hc would follow D^2 type behavior rather than D^6, as pointed out by Hoffmann *et al.*[51] The observed decrease in Hc, for the sample prepared in the presence of 2% nitrogen partial pressure, can be understood accordingly.

On the other hand, when nitrogen partial pressure was increased to 10%, the alloy formed an amorphous structure and the magnetic measurements showed a decrease in Ms as well as Hc. A decrease in Hc can be understood within RAM, when averaging is done on very fine grains and magnetization follows the easy direction of each individual grain. The decrease in the value of Ms can be understood due to weakening of the exchange coupling between the grains. Further, at R_{N_2}=20%, the Hc increase abruptly while Ms continues to decrease. It may be noted that at this nitrogen partial pressure, the amorphous phase coexists with the hcp-ϵ-Fe_3N phase. In case the ϵ-Fe_3N phase is nonferromagnetic (as found at higher R_{N_2}), the presence of a nonferromagnetic phase among the ferromagnetic fine grains would result in a decrease in exchange length, which, in accordance with the RAM, causes anisotropy and coercivity to increase because of incomplete averaging-out of random anisotropies of grains within the exchange volume. The observed increase in the Hc and decrease in Ms can be understood with this argument. At still higher nitrogen partial pressure where the ϵ-Fe_3N phase along with the ζ-Fe_2N phases were obtained, the magnetization was almost zero, indicating the nonferromagnetic nature of the film at this nitrogen pressure. The films deposited at even higher R_{N_2} were also nonferromagnetic.

Crystallization behavior of the amorphous film deposited at R_{N_2}=10% was also studied with magnetization measurements of the samples annealed at different temperatures. Figure 10 shows magnetization measurements after annealing at

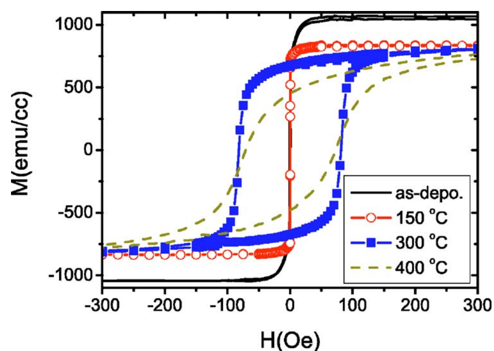

FIG. 10. (Color online) Magnetization measurements of FeN thin film prepared at 10% nitrogen partial pressure as a function of annealing temperature.

different temperatures as discussed in the previous section. The M-H loop shape up before crystallization temperature was similar to that in the as-deposited state. The only appreciable change was the shape of the M-H loop, which became more square after annealing. Such a change in the M-H loop shape is directly related to the removal of strains which might have developed during the deposition. At higher annealing temperature where crystallization of the amorphous phase takes place, the loop shape was completely different. There was a sharp increase in the value of coercivity and the average value of Ms decreased. At still higher temperature, the value of Ms further decreased and the loop shape is broader. From the XRD measurements, it is evident that upon crystallization ϵ-Fe_3N phase precipitates out and an increase in the Hc and decrease in Ms is similar as observed for the sample prepared at $R_{N_2}=20\%$, where the ϵ-Fe_3N phase existed. The observed magnetization behavior can be understood accordingly.

The magnetization measurements were also carried out in NiFeN films as a function of nitrogen partial pressure during sputtering. The M-H loop for the sample prepared with Ar gas only is matching well with the values obtained for permalloy.[52] For the samples prepared with increased R_{N_2}, the magnetization decreased rapidly and the values of coercivity increased (see Fig. 11). As will be discussed later, the start structure with NiFe is fcc, and the volume of the interstitial is much larger in the case of fcc as compared with a bcc Fe. This allows more nitrogen atoms to be incorporated

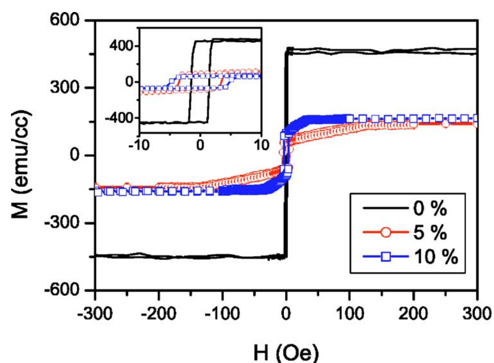

FIG. 11. (Color online) Magnetization measurements of NiFeN thin films prepared at different nitrogen partial pressures.

within the unit cell of fcc NiFe, which eventually results in a decrease in magnetization more rapidly as compared with bcc Fe. The observed magnetization behavior may be understood with this argument.

F. Polarized neutron reflectivity measurements

In the present case, since the samples were deposited either on glass or Si substrate and the thickness of the deposited films was in the range of 100 nm, the diamagnetism of the substrates might result in erroneous values of absolute saturation magnetization when measured with a dc extraction magnetometer. Also, the errors in determining the size of the measured samples may lead to further errors in the values of absolute magnetization. With these two parameters in mind, the magnetization of the FeN samples was also determined using polarized neutron reflectivity (PNR). PNR is a technique which is able to yield the absolute value of a magnetic moment per atom in a magnetic thin film with high accuracy.[53] In contrast to the bulk magnetization magnetometer technique (e.g., dc extraction, VSM, or SQUID), no correction due to the magnetic signal from the substrate has to be applied in PNR. Further, the sample dimensions and mass do not play a crucial role in the determination of the magnetic moment. During the experiment, polarized neutrons with spin parallel or antiparallel to the direction of magnetization on the sample are reflected off the surface of the sample at grazing incidence. The measurements were performed with an applied field of 400 Oe, which is sufficient to reach the saturation magnetization in all the samples. The measurements were carried out in the TOF mode at a fixed angle of incidence. The TOF-PNR has an advantage as during the measurement of spin-up and spin-down reflectivities, only the polarization of the incoming beam is changed by switching the direction of the applied field at the polarizing supermirror.[36] No movement of the sample is required as is often done in the θ-2θ mode. The potential energy of a neutron in the ith region of the sample is given by[53,54]

$$V_i = \frac{2\pi\hbar^2}{m_n}\rho_i b_i + \mu_n \cdot B_i, \qquad (2)$$

where m_n, ρ_i, b_i, μ_n, and B_i are the mass of a neutron, the atomic density, the coherent scattering length, the neutron moment, and the magnetic field. This potential gives rise to spin-dependent reflectivity for the cases when incident polarization is parallel to the direction of magnetization in the sample (+) or antiparallel (−). Figure 12 shows PNR data on the samples prepared as a function increased nitrogen partial pressure during sputtering. As the amount of nitrogen partial pressure is increased, the edge in $R-$ shows a shift towards higher q_z values, and the separation between $R+$ and $R-$ reflectivities decreases continuously. Finally, for $R_{N_2} > 20$, both $R+$ and $R-$ are merged together, indicating that the sample has became nonferromagnetic. The magnetic moment in each case was determined by fitting the experimental data using a computer program.[55] Figure 13 shows a plot of obtained values of the magnetic moment with PNR and bulk magnetization measurements. Perusal of the figures gives a clear indication that the values of the magnetic moment ob-

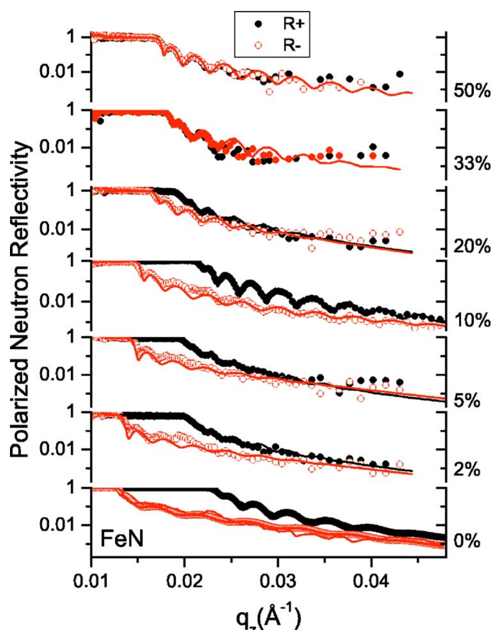

FIG. 12. (Color online) Polarized neutron reflectivity measurements of FeN thin films prepared at different nitrogen partial pressures. Closed circles represents the data corresponding to spin-up reflectivity $R+$ and open circles to spin-down reflectivity $R-$. The solid line represents fitting to the experimental data.

tained with the two techniques lie in the same range within the experimental errors. It is interesting to note that at no point is the magnetic moment higher than that of bulk Fe.

IV. MECHANISM INDUCING NANOCRYSTALLIZATION OR AMORPHIZATION

From the results and discussion given in the previous section, it is clear that both Fe and NiFe form a nanocrystalline or amorphous structure when sputtered with reactive nitrogen. Only at some specific nitrogen partial pressures are polycrystalline structures obtained. The mechanism inducing nanocrystallization or amorphization can be understood in

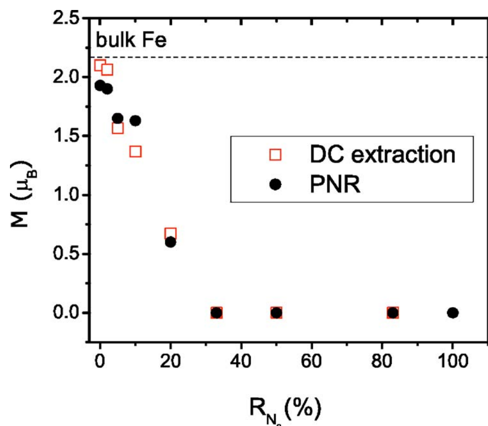

FIG. 13. (Color online) Magnetic moment as obtained with the bulk magnetization measurements and polarized neutron reflectivity.

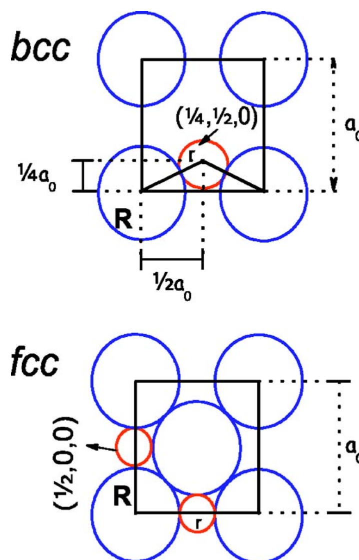

FIG. 14. (Color online) Distribution of the interstitial site in bcc and fcc structures.

terms of incorporation of nitrogen within the crystal structures of Fe and NiFe and rapid quenching of adatoms at the substrate. Atoms with low Z, e.g., B, C, or N, can easily occupy interstitial sites causing an expansion of the unit cell as well as restricting the long-range ordering. It may be noted that for Fe the structure is bcc, while for NiFe it is fcc. The probability of occupying the interstitial sites in the bcc and fcc crystal system is different because of different close packing. In bcc Fe, the atoms may occupy the tetrahedral interstitial sites (see Fig. 14), such as $(\frac{1}{4},\frac{1}{2},0)$, while in a fcc structure, nitrogen atoms may be located either at the octahedral sites at the edge center of the unit cell $(\frac{1}{2},0,0)$ and/or at the center of the unit cell $(\frac{1}{2},\frac{1}{2},\frac{1}{2})$. The probability of occupation of nitrogen atoms at the interstitial sites in the two structures can be obtained by calculating the size of the interstitials for the two cases:

The radius of the tetrahedral interstitial site at $(\frac{1}{4},\frac{1}{2},0)$, location in bcc Fe can be written as

$$r_{\mathrm{int}}=\left[\left(\tfrac{1}{2}a_0\right)^2+\left(\tfrac{1}{4}a_0\right)^2\right]^{1/2}-R_{\mathrm{bcc}}, \tag{3}$$

where R_{bcc} is the radius of bcc Fe and a_0 (=0.2866 nm) is the lattice constant of the bcc Fe atom and $R_{\mathrm{bcc}}=\sqrt{3}a_0/4$ =0.1241 nm. From Eq. (3), the radius of $(\frac{1}{4},\frac{1}{2},0)$ location of the interstitial site r_{int} for bcc Fe is 0.0361 nm. Similarly, we can calculate the radius of the interstitial site for fcc NiFe at the octahedral sites $(\frac{1}{2},0,0)$ using the expression

$$2r_{\mathrm{int}}=a_0-2R_{\mathrm{fcc}}, \tag{4}$$

where a_0=0.3545 nm for NiFe and R_{fcc} is the radius of fcc NiFe and $R_{\mathrm{fcc}}=\sqrt{2}a_0/4$=0.1253 nm. From Eq. (4), the radius of the $(\frac{1}{2},0,0)$ location of the interstitial site r_{int} for fcc is 0.0523 nm.

The interstitial site in the bcc Fe is smaller than that in the fcc NiFe alloy, whereas both are smaller than the atomic radius of a nitrogen atom (0.075 nm). Therefore, for both Fe and NiFe, nitrogen occupying the interstitial sites would

cause a distortion to the unit cell, and it is expected that this distortion should be more effective for bcc Fe as compared with fcc NiFe while depositing at a given nitrogen partial pressure. As a matter of fact, it is clear from our XRD results that almost complete amorphization of Fe was observed at $R_{N_2}=10\%$, while in the case of NiFe, a fully amorphous state was obtained at $R_{N_2}=33\%$. This result clearly indicated that nitrogen atoms gradually occupy the interstitial space within bcc or fcc structure, and since available space in a fcc structure is larger, fcc structure allowed more nitrogen atoms to be incorporated. Further, when nitrogen partial pressure was increased beyond the one at which final amorphous structure was obtained, the structure of both Fe and NiFe was changed basically to A_3N (A=Fe or NiFe).

From the energetics of binary iron nitrides[56] (at room temperature), it may be noted that the heat of formation for ϵ-Fe_3N_x is lower (-40 to -45 kJ mol^{-1}) as compared with neighboring, e.g., Fe_4N (-12 kJ mol^{-1}) or Fe_2N (-34 kJ mol^{-1}), phases. On the other hand, the nitrogen-richest phase γ'''-$FeN_{0.91}$ has the lowest enthalpy of formation (-47 kJ mol^{-1}). It is expected that at intermediate nitrogen pressures when no more interstitial nitrogen can be incorporated within the unit cell, Fe_3N or Fe_2N phases would be readily formed. In fact, when sputtered with $R_{N_2}=33\%$, iron nitride structure is a mixture of Fe_3N and Fe_2N phases. Further increase in nitrogen partial pressure at 50% resulted in the formation of nitrogen-rich γ'''-type FeN. Still, since the peaks were broadened, completely crystalline structure was not formed. At $R_{N_2}=83\%$, sharp reflections corresponding to γ'''-FeN were observed. A further increase in the nitrogen partial pressure resulted in broadening of the XRD peaks. This means that well-defined polycrystalline structure of FeN compounds is only obtained at some specific nitrogen partial pressures, and below and above these specific partial pressures the long-range ordering is restricted due to incomplete Fe-N bonds or partial breaking of Fe—N bonds due to excessive nitrogen. Similar behavior was also observed for NiFe, however the amount of incorporation of nitrogen atoms in the two cases is different.

The energy of the adatoms with parameters used during sputtering for Fe or NiFe would be around 10 eV,[57] which corresponds to roughly 10^5 K. During condensation onto the substrate which tales place within ~ms, the adatoms are rapidly quenched and the mobility of the atoms is restricted; it is expected that either the occupancy of reactive nitrogen at interstitial sites or a chemical reaction between a sputtered atom and nitrogen takes place in the plasma. Since the substrate was not heated intentionally, it is very unlikely that any rearrangement process would take place onto the substrate after condensation. This argument supports the idea that the microstructure of the deposited film would strongly depend on the plasma, which in turn depends upon the amount of reactive nitrogen used during sputtering. Since nitrogen atoms gradually occupy interstitial sites in Fe or NiFe, it is expected that the microstrain of the structure should increase as the amount of nitrogen partial pressure is increasing. The microstrain variation in the samples studied in the present case can be determined from XRD data using Williamson-Hall plots for the Lorentzian peak shape,[58]

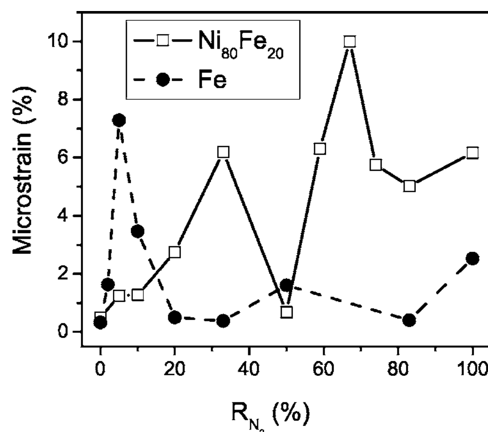

FIG. 15. Microstrain obtained from the XRD data (see Fig. 1 and Fig. 4) for FeN and NiFeN samples prepared with different nitrogen partial pressures. The solid and dotted lines are a guide to the eye.

$$b \cos \theta = A + B \sin \theta, \tag{5}$$

where $A=0.9\lambda/t$, t is the grain size, $B=4\epsilon$(ϵ=microstrain), and b is the full width at half maximum in 2θ.

A straight line fit in the plot of $b \cos \theta$ and $\sin \theta$ yields the values of constant A and B, which in turn yield the values of grain size as well as microstrain. Such a plot was obtained for all the sample displayed in Fig. 1 and Fig. 4. The obtained values of microstrain for FeN and NiFeN are plotted in Fig. 15. It may be noted that the higher-order reflections in the present case are reflected poorly; effective microstrain can be obtained using the most intense peak.[59] Further, the microstrain in the deposited samples can have another origin, such as grain size or dislocation. However, a comparison of microstrain for the samples prepared at different nitrogen partial pressure is expected to provide additional insight into the mechanism inducing nanocrystallization or amorphization. It is interesting to see that for both FeN and NiFeN the microstrain is largest for the amorphous phases, while for polycrystalline phases of nitrides or pure Fe and NiFe it is almost zero. An increase in the microstrain on nanocrystallization and amorphization gives an indication that the unit cell of Fe or NiFe is distorted due to incorporation of nitrogen at interstitial sites. Whenever a polycrystalline structure is formed, the microstrain is at a minimum. Since the polycrystalline structure is formed due to almost complete covalent bonds between Fe and N or NiFe and N, the distortion of the unit cell should be at a minimum. An incomplete bonding or excessive nitrogen increased the microstrain in the film, which leads to a nanocrystalline or amorphous phase of the deposited sample. This argument, combined with the fact that adatoms are quenched at the substrate within a very short time, explains the mechanism inducing nanocrystallization or amorphization. Even though amorphization or nanocrystallization increased the microstrain within the structure of the deposited film, it is interesting to note that the surface roughness of the amorphous film was improved on amorphization, which gives an indication that strains are developed within the structure.

V. CONCLUSIONS

From the present study, it can be concluded that reactive nitrogen sputtering of bcc Fe and fcc NiFe (at room temperature) forms a nanocrystalline or amorphous structure at most of the nitrogen partial pressures. Only at specific nitrogen partial pressures were polycrystalline nitrides obtained which are thermodynamically favored. Above or below this specific pressure, the long-range ordering is perturbed by reactive nitrogen. The crystallization in both amorphous FeN and NiFeN takes place in a single step, and at higher temperature nitrogen-poor phases are formed due to nitrogen out-diffusion. The growth behavior of amorphous FeN showed improved surface roughness due to amorphization and the growth exponent β was minimum for the amorphous phase as compared with poly or nanocrystalline phases. The magnetic measurements on ferromagnetic FeN and NiFeN films reveal that in the case of FeN, at low nitrogen content, the alloy forms a soft-magnetic phase, while at higher nitrogen content the average value of magnetization decreased and coercivity increased. For NiFeN, inclusion of nitrogen produced phases with reduced values of magnetization. The magnetic moment of the samples was confirmed with polarized neutron reflectivity and was in agreement with the values obtained with dc extraction magnetometery.

ACKNOWLEDGMENTS

We are grateful to Michael Horisberger for providing help with thin film deposition and Dr. Yu Lung Chiu for TEM measurements. One of the authors (R.G.) would like to thank Dr. Peter Allenspach for his support and for making available the experimental facilities at the Laboratory for Neutron Scattering, Paul Scherrer Institut. Part of this work was performed at the Swiss Spallation Neutron Source, Paul Scherrer Institut, Villigen, Switzerland.

*Electronic address: mukul.gupta@psi.ch

[1] C. A. Angell, K. L. Ngai, G. B. McKenna, P. F. McMillan, and S. W. Martin, J. Appl. Phys. **88**, 3113 (2000).
[2] P. G. Debenedetti and F. H. Stillinger, Nature (London) **410**, 259 (2001).
[3] M. E. McHenry, M. A. Willard, and D. E. Laughlin, Prog. Mater. Sci. **44**, 291 (1999).
[4] A. Dunlop, G. Jaskierowicz, G. Rizza, and M. Kopcewicz, Phys. Rev. Lett. **90**, 015503 (2003).
[5] C. Line, D. Sun, S. L. Ming, E. Jiang, and Y. Liu, Thin Solid Films **279**, 49 (1996).
[6] N. Sulitanu and F. Brinza, J. Optoelectron. Adv. Mater. **5**, 421 (2003).
[7] F. Faupel, W. Frank, M. P. Macht, H. Mehrer, K. Rätzke, H. Schober, S. K. Sharma, and H. Teichler, Rev. Mod. Phys. **75**, 237 (2003).
[8] S. R. Elliott, *Physics of Amorphous Materials*, 2nd ed. (Longman Scientific and Technical, Harlow, Essex, 1990).
[9] C. C. Koch, O. B. Cavin, C. G. McKamey, and J. O. Scarbrough, Appl. Phys. Lett. **43**, 1017 (1983).
[10] W. J. Meng, P. R. Okamoto, L. J. Thompson, B. J. Kestel, and L. E. Rehn, Appl. Phys. Lett. **53**, 1820 (1988).
[11] S. M. Sharma and A. K. Sikka, Prog. Mater. Sci. **40**, 1 (1996).
[12] R. B. Schwarz and W. L. Johnson, Phys. Rev. Lett. **51**, 415 (1983).
[13] W. L. Johnson, Prog. Mater. Sci. **28**, 229 (1985).
[14] K. Samwer, Phys. Rep. **161**, 1 (1988).
[15] M. Holz, P. Ziemann, and W. Buckel, Phys. Rev. Lett. **51**, 1584 (1983).
[16] S. Takeda and J. Yamasaki, Phys. Rev. Lett. **83**, 320 (1999).
[17] N. Hellgren, M. P. Johansson, E. Broitman, L. Hultman, and J.-E. Sundgren, Phys. Rev. B **59**, 5162 (1999).
[18] D. Babonneau, M. Jaouen, M.-F. Denanot, P. Guérin, and F. Petroff, Appl. Phys. Lett. **82**, 3056 (2003).
[19] M. Gupta, A. Gupta, S. Rajagopalan, and A. K. Tyagi, Phys. Rev. B **65**, 214204 (2002).
[20] A. Gupta, M. Gupta, B. A. Dasannacharya, S. Kikuta, Y. Yoda, and M. Seto, J. Phys. Soc. Jpn. **73**, 423 (2004).
[21] L. Rissanen, M. Neubauer, K. P. Lieb, and P. Schaaf, J. Alloys Compd. **274**, 74 (1998).
[22] M. A. Russak, C. V. Jahnes, E. Klokholm, J.-W. Lee, M. E. Re, and B. C. Webb, J. Appl. Phys. **70**, 6427 (1991).
[23] J.-F. Bobo, H. Chatbi, M. Vergnat, L. Hennet, O. Lenoble, P. Bauer, and M. Piecuch, J. Appl. Phys. **77**, 5309 (1995).
[24] H. B. Nie, S. X. Xu, C. K. Ong, Q. Zhan, D. X. Li, and J. P. Wang, Thin Solid Films **440**, 35 (2003).
[25] T. Stobiecki, M. Kopcewicz, W. Powroźnik, E. Kusior, P. Wiśniowski, W. Maass, B. Ocker, and H. Rohrmann, J. Magn. Magn. Mater. **240**, 448 (2002).
[26] T. Yoshitake and M. Ohkoshi, IEEE Trans. Magn. **31**, 3850 (1995).
[27] M. Gupta, A. Gupta, P. Bhattacharya, P. Misra, and L. M. Kukreja, J. Alloys Compd. **326**, 265 (2001).
[28] N. Wang, K. M. Ulmer, P. A. Constant, J. W. Anderegg, and J. E. Snyder, J. Vac. Sci. Technol. A **21**, 1734 (2003).
[29] L. Guibin, L. Guoqing, L. Minaki, and L. Bangzhi, Surf. Coat. Technol. **96**, 34 (1997).
[30] T. Kim and M. Takahashi, Appl. Phys. Lett. **20**, 492 (1972).
[31] Y. D. Zhang, J. I. Budnick, W. A. Hines, M. Q. Huang, and W. E. Wallace, Phys. Rev. B **54**, 51 (1996).
[32] C. Chang, J. M. Sivertsen, and J. H. Judy, IEEE Trans. Magn. **MAG 23**, 3636 (1987).
[33] X. Wang, W. T. Zheng, H. Tian, S. S. Yu, and L. L. Wang, J. Magn. Magn. Mater. **283**, 282 (2004).
[34] M. Chiba, K. Morio, and Y. Koizumi, J. Magn. Magn. Mater. **242**, 949 (2002).
[35] M. Kawamura, Y. Abe, and K. Sasaki, Vacuum **59**, 721 (2000).
[36] M. Gupta, T. Gutberlet, J. Stahn, P. Keller, and D. Clemens, Pramana, J. Phys. **63**, 57 (2004).
[37] B. D. Cullity, *Elements of X-ray Diffraction* (Addison-Wesley, Reading, MA, 1978).
[38] A. Guinier, *X-Ray Diffraction: In Crystals, Imperfect Crystals and Amorphous Bodies* (Dover, New York, 1994).
[39] K. Hono and D. H. Ping, Mater. Charact. **44**, 203 (2000).

[40] D. M. Zhu, K. Raviprasad, K. Suzuki, and S. P. Ringer, J. Phys. D **37**, 645 (2004).
[41] C. Braun, *Parratt32—The Reflectivity Tool* (HMI, Berlin, 1997–99).
[42] L. G. Parratt, Phys. Rev. **95**, 359 (1954).
[43] A. L. Barabási and H. E. Stanley, *Fractal Concepts in Surface Growth* (Cambridge University Press, Cambridge, UK, 1995).
[44] M. Lütt, J. P. Schlomka, M. Tolan, J. Stettner, O. H. Seeck, and W. Press, Phys. Rev. B **56**, 4085 (1997).
[45] M. Kardar, G. Parisi, and Y.-C. Zhang, Phys. Rev. Lett. **56**, 889 (1986).
[46] G. Herzer, IEEE Trans. Magn. **25**, 3327 (1989).
[47] G. Herzer, IEEE Trans. Magn. **26**, 1397 (1990).
[48] J. F. Löffler, J. P. Meier, B. Doudin, J.-P. Ansermet, and W. Wagner, Phys. Rev. B **57**, 2915 (1998).
[49] R. W. Gao *et al.*, J. Appl. Phys. **94**, 664 (2003).
[50] J. F. Löffler, H.-B. Braun, and W. Wagner, Phys. Rev. Lett. **85**, 1990 (2000).
[51] H. Hoffmann and T. Fujii, J. Magn. Magn. Mater. **128**, 395 (1993).
[52] B. D. Cullity, *Introduction to Magnetic Materials* (Addison-Wesley, Reading, MA, 1972).
[53] S. J. Blundell and J. A. C. Bland, Phys. Rev. B **46**, 3391 (1992).
[54] S. Hope *et al.*, Phys. Rev. B **55**, 11 422 (1997).
[55] F. Ott, SIMULREFLEC, http://www-llb.cea.fr/prism/programs/simulreflec/simulreflec.html.
[56] F. Tessier, A. Navrotsky, R. Niewa, A. Leineweber, H. Jacobs, S. Kikkawa, M. Takahashi, F. Kanamaru, and F. J. DiSalvo, Solid State Sci. **2**, 457 (2000).
[57] G. M. Turner, I. S. Falconer, B. W. James, and D. R. McKenzie, J. Vac. Sci. Technol. A **10**, 455 (1992).
[58] Y. Rosenberg, V. S. Machavariani, A. Voronel, S. Garber, A. Rubshtein, A. I. Frenkel, and E. A. Stern, J. Phys.: Condens. Matter **12**, 8081 (2000).
[59] L. R. Shaginyan, M. Misina, J. Zemek, J. Musil, F. Regent, and V. F. Britun, Thin Solid Films **408**, 136 (2002).